Digital Signal Processing 34 (2014) 48–55

Contents lists available at ScienceDirect

Digital Signal Processing

www.elsevier.com/locate/dsp

High accuracy and low complexity adaptive Generalized Sidelobe Cancelers for colored noise scenarios

Ricardo Kehrle Miranda [a], João Paulo C.L. da Costa [a], Felix Antreich [b]

[a] Laboratory of Array Signal Processing (LASP), Department of Electrical Engineering, University of Brasília, Brazil
[b] Institute of Communications and Navigation, German Aerospace Center (DLR), Germany

ARTICLE INFO

Article history:
Available online 30 July 2014

Keywords:
Beamforming
Array processing
Colored noise
Prewhitening

ABSTRACT

The Generalized Sidelobe Canceler (GSC) is a beamforming scheme which is applied in many fields such as audio, RADAR, SONAR and telecommunications. Recently, the adaptive Reduced Rank GSC (RR-GSC) has been proposed for applications with a large number of sensors. Due to its dimensionality reduction step, the adaptive RR-GSC achieves an enhanced performance in comparison with the standard GSC. However, both standard GSC and RR-GSC have their performance drastically degraded in the presence of colored noise.

In this paper, we propose to extend further the GSC and the RR-GSC for colored noise scenarios. As shown in this paper, such improvement in colored noise scenarios can be obtained by incorporating a stochastic or a deterministic prewhitening step in the GSC and RR-GSC algorithms. Since the prewhitening increases the computational complexity, a block-wise reduced rank stochastic gradient GSC beamformer is also proposed. The block-wise step allows only one prewhitening step per block while in the previous schemes one per sample was needed. Another proposed advance in colored noise scenarios is the incorporation of the Vandermonde Invariance Transform (VIT). The VIT works as a pre-beamformer which reduces the interferent power of the undesired sources and the colored noise effect. We show by means of simulations the improved results even for highly correlated scenarios.

1. Introduction

Beamforming is an important topic in array signal processing and has applications in several fields such as RADAR [1], SONAR [2], telecommunications [3] and audio [4]. In the literature, there are several adaptations of Direction of Arrival (DOA) estimation schemes for colored noise scenarios [5–7], and once the DOA information is obtained, it can be introduced to the beamformer. The addition of such constraints led to the development of beamformers such as the Direct Form Processor (DFP), which includes the Linearly Constrained Minimum Variance (LCMV) and Linearly Constrained Constant Modulus (LCCM) [8], and the Generalized Sidelobe Canceler (GSC) [9]. For real time applications, the necessity for adaptive algorithms grows and, with this need, adaptive versions of the GSC were proposed in earlier works [10,11,8].

However, when the number of elements in a sensor array is high, these algorithms suffer from computational complexity increase. Therefore, recently, adaptive reduced rank DFP and GSC schemes were also proposed in order to reduce the dimensionality of the adaptive filters. The rank reduction step also has a noise removal effect, thus showing an enhanced performance [11,8]. These works use the constant modulus (CM) cost function [10], as it was shown to have a better accuracy for constant envelope signals. Yet, adaptive beamforming techniques using the GSC usually assume uncorrelated white noise in the receivers, which is not realistic.

For colored noise scenarios, prewhitening schemes have been successfully applied in combination with DOA estimation [5,6] and audio signal processing schemes [12]. The prewhitening schemes are divided into stochastic [6,12] and deterministic prewhitening [5]. In deterministic prewhitening, the noise may have a specific structure which can be exploited, while in the stochastic prewhitening, no structure is assumed. Moreover, there are also multidimensional prewhitening schemes for the case that the data has a tensor structure [13].

In this work, we propose to extend the least mean squares GSC (LMS-GSC) and the Reduced Rank LMS-GSC (RR-LMS-GSC) for colored noise scenarios by incorporating a prewhitening step. We propose the prewhitened GSC schemes considering the deterministic prewhitening [5] and the stochastic prewhitening [6,12]. The colored noise is usually concentrated in certain direction. Therefore,

E-mail addresses: rickehrle@unb.br (R.K. Miranda), joaopaulo.dacosta@ene.unb.br (J.P.C.L. da Costa), felix.antreich@dlr.de (F. Antreich).
URL: http://www.redes.unb.br/lasp (R.K. Miranda).

http://dx.doi.org/10.1016/j.dsp.2014.07.015

to further enhance the GSC, the VIT [14] is also applied as a preprocessing step. The colored noise can be also concentrated close to the desired signal direction, therefore a prewhitening step is also still needed along the VIT. The stochastic prewhitening needs the computation of one SVD at each iteration. In order to reduce the complexity of the stochastic prewhitening, we propose the block-wise reduced rank stochastic gradient GSC (BW-RR-GSC) beamformer.

This paper is divided into 6 sections including this introduction. In Section 2 we present the data model for colored noise. In Section 3 the classic beamformer designs for the LMS-GSC and RR-LMS-GSC are briefly introduced. Then, in Section 4 we propose our high accuracy and low complexity GSC schemes by incorporating prewhitening steps, the VIT and a block-wise modification for colored noise scenarios. In Section 5, simulations are shown and the results are drawn. Finally, Section 6 makes the conclusions about the work.

Notation Scalars are denoted by lower-case letters $(a, b, \ldots)$, vectors are written as boldface lower-case letters $(\mathbf{a}, \mathbf{b}, \ldots)$ and matrices as boldface capitals $(\mathbf{A}, \mathbf{B}, \ldots)$. The superscripts $^{\mathrm{T}}$, $^{\mathrm{H}}$ and * represent transpose, Hermitian transpose and complex conjugate of a term, respectively. The operator $\mathrm{E}\{\cdot\}$ stands for the expected value operation.

2. Data model

We assume that d sources are transmitting different symbols at the n-th time instant. Since the sources are far away from the receiver, the narrowband wave fronts are considered planar. We assume a Uniform Linear Array (ULA) with M isotropic sensor elements with an inter-element spacing of Δ wavelengths. Therefore, we can mathematically represent the received symbols as

$$\mathbf{x}(n) = \mathbf{a}(\theta_0)s(n) + \mathbf{A}_{\mathrm{int}}(\boldsymbol{\theta}_{\mathrm{int}})\mathbf{s}_{\mathrm{int}}(n) + \mathbf{n}^{(\mathrm{c})}(n), \tag{1}$$

where $\mathbf{x}(n) = [x_0(n), \ldots, x_{M-1}(n)]^{\mathrm{T}}$ is the vector containing the received symbols at time instant n, $s(n)$ is the desired signal, $\mathbf{s}_{\mathrm{int}}(n)$ is a vector with the interference symbols from the $d-1$ interferes and $\mathbf{n}^{(\mathrm{c})}(n)$ contains colored noise samples at the sensor elements. Note that $\mathbf{n}^{(\mathrm{c})}(n) = \mathbf{L}\mathbf{n}(n)$, where $\mathbf{n}(n)$ contains i.i.d. noise samples with Circularly Symmetric Complex Gaussian (CSCG) distributions. The matrix $\mathbf{L} \in \mathbb{C}^{M\times M}$ stands for the correlation matrix. For the special case where $\mathbf{L}$ is the identity matrix the noise becomes white at the sensors. The vector $\mathbf{a}(\theta_0)$ is the steering vector with a Vandermonde structure for the desired signal, where the elements of the vector $\mathbf{a}(\theta_0)$ are a function of the DOA of the desired signal defined as θ_0 and are arranged in a column. The matrix $\mathbf{A}_{\mathrm{int}}(\boldsymbol{\theta}_{\mathrm{int}}) \in \mathbb{C}^{M\times d-1}$ is the steering matrix containing all the steering vectors of the interfering signals where their corresponding DOAs are comprised in the vector $\boldsymbol{\theta}_{\mathrm{int}} \in \mathbb{C}^{d-1\times 1}$. The DOAs might also be represented by the spatial frequencies, i.e. spatially related phase delays, $\phi_0 = -2\pi\,\Delta\sin\theta_0$ and $\boldsymbol{\phi}_{\mathrm{int}} = -2\pi\,\Delta\sin\boldsymbol{\theta}_{\mathrm{int}} \in \mathbb{C}^{d-1\times 1}$, respectively.

More generally, assuming a sliding window in which at time n a snapshot of the current and the $N-1$ previously transmitted symbols are allocated into a vector $\mathbf{s}$ and collecting the interfering signals into a matrix $\mathbf{S}_{\mathrm{int}}(n) \in \mathbb{C}^{N\times d-1}$ we can rewrite our model in a compact format

$$\mathbf{X}(n) = \mathbf{a}(\theta_0)\mathbf{s}^{\mathrm{T}}(n) + \mathbf{A}_{\mathrm{int}}(\boldsymbol{\theta}_{\mathrm{int}})\mathbf{S}_{\mathrm{int}}^{\mathrm{T}}(n) + \mathbf{N}^{(\mathrm{c})} \in \mathbb{C}^{M\times N}, \tag{2}$$

where $\mathbf{X}(n) = [\mathbf{x}(n-N+1), \ldots, \mathbf{x}(n)]$ and $\mathbf{N}^{(c)} = \mathbf{L}\cdot\mathbf{N} \in \mathbb{C}^{M\times N}$. The matrix $\mathbf{N} \in \mathbb{C}^{M\times N}$ contains the N white noise samples for all M sensors in the same manner as $\mathbf{X}$ contains N signal plus noise samples from the M sensors. The variable $\mathbf{s}(n) \in \mathbb{C}^{N\times 1}$ has the N latest samples for the desired signal and $\mathbf{S}_{\mathrm{int}} \in \mathbb{C}^{N\times d-1}$ has the N latest samples for the $d-1$ interfering sources.

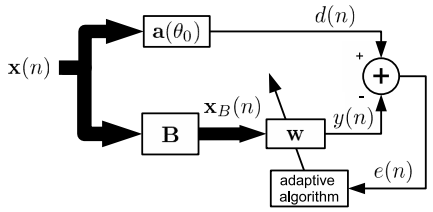

Fig. 1. LMS-GSC block diagram.

Here, we assume that the received symbols $\mathbf{X}(n)$ and the DOA of the desired signal θ_0 are known at the receiver and we desire to find $\hat{s}(n)$, which is an estimate of $s(n)$. To find the DOA, we refer to [5–7] or alternatively we can assume that the position of the transmitter with respect to the receiver is known.

3. State-of-the-art beamformer designs

This section is divided into two subsections. In Section 3.1, we review the standard LMS-GSC beamformer, while in Section 3.2, we review the reduced rank LMS-GSC (RR-LMS-GSC).

3.1. LMS-GSC

The GSC algorithm turns a constrained problem into an unconstrained problem by introducing a blocking matrix, which is the orthogonal complement of the constraint $\mathbf{a}(\theta_0)$. In our case, the constraint is formed based on the steering vector of the desired signal, which can be estimated via [5–7].

In Fig. 1, the input signal $\mathbf{x}(n)$ passes through a beam pointed at the desired signal direction θ_0 generating $d(n) = \mathbf{a}^{\mathrm{H}}(\theta_0)\mathbf{x}(n)$. The same input signal also passes through a blocking matrix $\mathbf{B}$ which is the orthogonal complement of the constraint $\mathbf{a}(\theta_0)$. Consequently, $\mathbf{B}$ blocks the desired signal and let ideally only $\mathbf{A}_i(\theta_i)\mathbf{s}_i(n)$ pass. The filter $\mathbf{w}$ should then be adjusted so that it generates the interference signal $y(n)$ that is subtracted from the desired signal $d(n)$.

In Fig. 1, $y(n)$ is given by

$$y(n) = \mathbf{w}^{\mathrm{H}}\mathbf{x}_B(n), \tag{3}$$

where $\mathbf{x}_B(n) = \mathbf{B}\mathbf{x}(n)$. As shown in Fig. 1, the error signal $e(n)$ is used by the adaptive algorithm to adjust $\mathbf{w}$. Once $\mathbf{w}$ converges, then we have that $\hat{s}(n) = e(n)$. Since $e(n)$ is free from interference it is also the system's output signal.

The adaptation of $\mathbf{w}$ is computed via stochastic gradient of the following cost function

$$J_{\mathrm{lms}}(\mathbf{w}) = E\left\{\left|d(n) - \mathbf{w}^{\mathrm{H}}\mathbf{x}_B(n)\right|^2\right\} \tag{4}$$

which gives the update rule for the adaptive part

$$\mathbf{w}(n+1) = \mathbf{w}(n) + \mu_{\mathrm{lms}}\nabla_{\mathbf{w}}J_{\mathrm{lms}}(\mathbf{w}) \tag{5}$$

with μ_{lms} being the step size for the LMS-GSC.

We use the instantaneous estimates $\hat{\mathbf{R}}_{\mathbf{xx}} = \mathbf{x}(n)\mathbf{x}^{\mathrm{H}}(n)$ and $\hat{\mathbf{r}}_{d\mathbf{x}} = d(n)\mathbf{x}(n)$ [9] to find the stochastic gradient:

$$\hat{\nabla}_{\mathbf{w}}J_{\mathrm{lms}} = 2\mathbf{B}\mathbf{x}(n)\mathbf{x}^{\mathrm{H}}(n)\mathbf{B}^{\mathrm{H}}\mathbf{w} - 2\mathbf{B}d(n)\mathbf{x}(n). \tag{6}$$

Now the stochastic gradient is inserted into LMS update rule for the GSC [9]:

$$\mathbf{w}(n+1) = \mathbf{w}(n) + \mu_{\mathrm{lms}}\mathbf{B}\mathbf{x}(n)\mathbf{x}^{\mathrm{H}}(n)\left(\mathbf{a}(\theta_0) - \mathbf{B}^{\mathrm{H}}\mathbf{w}\right). \tag{7}$$

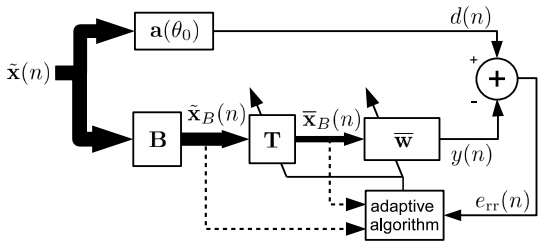

Fig. 2. RR-LMS-GSC block diagram.

3.2. RR-LMS-GSC

Regular LMS algorithms have been reported to have a slow convergence for high number of sensor elements M [11]. To overcome these drawbacks, a reduced rank (RR) adaptive algorithm for the GSC scheme was developed in [8,11] and is depicted in Fig. 2. The process is similar to that described in Section 3.1, except that the blocked signal passes through a transformation matrix $\mathbf{T} \in \mathbb{C}^{(M-1)\times r}$ that performs a dimensionality reduction. As derived in [10], $\tilde{\mathbf{x}}(n) = e^*_{\mathrm{rr}}(n)\mathbf{x}(n)$ is used instead of $\mathbf{x}(n)$ for the input signal, where $e_{\mathrm{rr}}(n) = \mathbf{w}^{\mathrm{H}}(n)\mathbf{x}(n)$ is the output signal for the RR algorithm as indicated by the subscript and $\mathbf{w}(n) = \mathbf{a}(\theta_0) - \mathbf{B}^{\mathrm{H}}\mathbf{T}(n)\overline{\mathbf{w}}(n)$. The CM error and its quadratic mean describes the CM cost function:

$$J_{\mathrm{cm}}(\mathbf{w}) = E\left\{\left|\mathbf{w}^{\mathrm{H}}\tilde{\mathbf{x}}(n) - \nu\right|^2\right\}, \tag{8}$$

where ν is constant set to 1 for unit variance signals. The filter $\mathbf{w}$ can be represented in terms of time evolving $\mathbf{T}(n)$ and $\overline{\mathbf{w}}(n)$ for the adaptation process. Thus, the expanded cost function becomes

$$J_{\mathrm{cm}}\big(\mathbf{T}(n), \overline{\mathbf{w}}(n)\big) = E\left\{\left|\left[\mathbf{a}(\theta_0) - \mathbf{B}^{\mathrm{H}}\mathbf{T}(n)\overline{\mathbf{w}}(n)\right]^{\mathrm{H}}\tilde{\mathbf{x}}(n) - \nu\right|^2\right\}, \tag{9}$$

with $\overline{\mathbf{w}}(n)$ being the reduced rank filter of size $r < M$. The stochastic gradient of the previous cost function with respect to $\mathbf{T}(n)$ and $\overline{\mathbf{w}}(n)$ gives their LMS update rules respectively

$$\mathbf{T}(n+1) = \mathbf{T}(n) + \mu_{\mathrm{T}} e^*_{\mathrm{cm}}(n)\tilde{\mathbf{x}}_{\mathbf{B}}(n)\overline{\mathbf{w}}^{\mathrm{H}}(n), \tag{10}$$

$$\overline{\mathbf{w}}(n+1) = \overline{\mathbf{w}}(n) + \mu_{\overline{\mathrm{w}}} e^*_{\mathrm{cm}}(n)\bar{\mathbf{x}}_{\mathbf{B}}(n), \tag{11}$$

where $e_{\mathrm{cm}} = 1 - \mathbf{w}(n)^{\mathrm{H}}\tilde{\mathbf{x}}(n)$ is the CM error. Also note that a new variable is introduced in (11) which corresponds to the filter input signal $\bar{\mathbf{x}}_{\mathbf{B}}(n) = \mathbf{T}^{\mathrm{H}}\tilde{\mathbf{x}}_{\mathbf{B}}(n)$, i.e. after the blocked signal transformation.

4. Proposed solutions

In this section, we propose different variations for the prewhitened adaptive GSC and prewhitened adaptive RR-GSC. The High Accuracy Stochastic Prewhitening (HASP) method that makes usage of one SVD per sample is shown in Section 4.1. The Vandermonde Invariant Transform (VIT) is also used along the HASP to create the VIT-HASP solution. In the phase perspective, the VIT keeps the Vandermonde structure in a desired direction and changes the directions of the interferent sources. From the spatial power sense, it acts as beamformer conserving power at a direction of interest and reduces the power in other directions. The VIT results in a virtual array that is further used by the adaptive GSC. Since the direction where the noise power is concentrated is not known, it can be close to the desired signal making the prewhitening still required, thus forming the VIT-HASP. In Section 4.3, the Deterministic Prewhitening (DP) method is shown for the cases where the correlation structure of the noise is known. Since the prewhitening step requires one SVD per sample for sample-wise adaptive algorithms, a new block-wise reduced rank stochastic gradient GSC beamformer (BW-RR-SG-GSC), which requires only one SVD per block, is also presented.

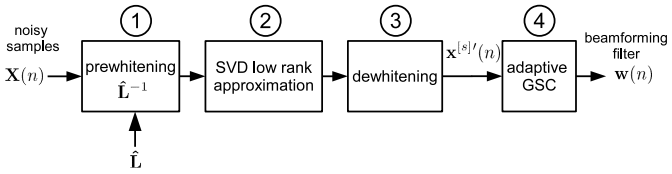

Fig. 3. High accuracy stochastic prewhitening block diagram.

4.1. High accuracy stochastically prewhitened LMS-GSC (HASP-LMS-GSC)

We start with the traditional stochastic prewhitening method for estimation of the noise correlation factor matrix and reduction of the effects of colored noise as proposed by [12]. First, we assume that samples are without signal components, i.e., only with noise, so that the noise sample correlation matrix can be given as

$$\hat{\mathbf{R}}_{\mathbf{NN}} = \frac{1}{N_{\mathrm{sf}}}\mathbf{N}^{(\mathrm{c})\prime} \cdot \left(\mathbf{N}^{(\mathrm{c})\prime}\right)^{\mathrm{H}}, \tag{12}$$

where N_{sf} stands for the number of signal free samples and $\mathbf{N}^{(\mathrm{c})\prime}$ is the colored noise snapshots matrix. Since $\hat{\mathbf{R}}_{\mathbf{NN}}$ is Hermitian and positive-definite we can perform the Cholesky decomposition

$$\hat{\mathbf{R}}_{\mathbf{NN}} = \hat{\mathbf{L}} \cdot \hat{\mathbf{L}}^{\mathrm{H}}, \tag{13}$$

with the estimated correlation factor matrix $\hat{\mathbf{L}}$ one can perform a prewhitening trying to revert the effects of the correlated noise in (1) by simply multiplying the data by the inverse of the estimated correlation factor matrix:

$$\mathbf{X}'(n) = \hat{\mathbf{L}}^{-1} \cdot \mathbf{X}(n), \tag{14}$$

where $\mathbf{X}'(n)$ is the prewhitened matrix of $\mathbf{X}(n)$. Once the number of signals d is known, we can apply an SVD low rank approximation on $\mathbf{X}'(n)$ resulting to $\mathbf{X}^{[s]}(n)$. We refer to the model order selection schemes [15–17] in order to estimate d. It is important to notice that this low rank approximation is not related to the rank reduction step performed by the adaptive algorithms. Finally, we separate the noise and signal subspace using the dewhitening step, which means multiplying it by the estimated correlation factor matrix $\hat{\mathbf{L}}$. This leads to the final input data:

$$\mathbf{X}^{[s]\prime}(n) = \hat{\mathbf{L}} \cdot \mathbf{X}^{[s]}(n). \tag{15}$$

In Fig. 3, (2) is used as input of the system for the HASP solution. Then, the SVD is applied in each iteration with the purpose of dewhitening. This results in a dewhitened data vector $\mathbf{x}^{[s]\prime}(n)$. The dewhitened data can now be inserted into the adaptive LMS-GSC or RR-LMS-GSC that will update the beamforming filter.

If the algorithm is element-wise adaptive, then only the latest dewhitened snapshot $\mathbf{x}^{[s]\prime}(n)$ is used at the iteration keeping in mind that $\mathbf{X}^{[s]\prime}(n) = [\mathbf{x}^{[s]\prime}(n-N+1), \cdots, \mathbf{x}^{[s]\prime}(n)]$. This snapshot can be directly inserted into the update rule (5) and update rules (11) and (10). The block-wise adaptation in Section 4.4 uses all the N snapshots.

4.2. Vandermonde Invariance Transformation (VIT) based HASP-LMS-GSC

The purpose of the VIT is to transform the input signal in a way that the Vandermonde structure is preserved [14]. Since there are always imperfections on the array, we refer to [18] for array interpolation in order to compensate such imperfections. First, we define a VIT matrix $\mathbf{T}_{\mathrm{vit}} \in \mathbb{C}^{M\times M}$ and multiplying it with a vector that has a Vandermonde structure $\mathbf{v} = [1, e^{j\phi}, \ldots, e^{j(M-1)\phi}]^{\mathrm{T}}$, [14] shows that

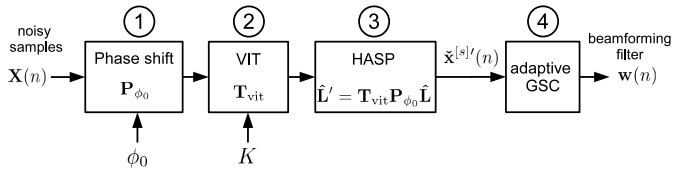

Fig. 4. VIT-HASP block diagram.

$$\check{\mathbf{v}} = \mathbf{T}_{\text{vit}} \cdot \mathbf{v} = \left(\frac{e^{j\phi} - \kappa}{1 - \kappa}\right)^{M-1} \cdot \begin{pmatrix} 1 \\ e^{j\nu} \\ \vdots \\ e^{j(M-1)\nu} \end{pmatrix}, \tag{16}$$

where κ is a complex parameter that originates a phase gain. From Eq. (16) it is inferred that the original phase ϕ is mapped into a new phase ν, but the Vandermonde structure is still present. More specifically, the new virtual phase is

$$\nu = \arctan\left(\frac{2K \cdot \sin\phi}{1 - K^2 + (1 + K^2) \cdot \cos\phi}\right), \tag{17}$$

where $K = (\kappa + 1)/(\kappa - 1)$. From (17) it is clear that the phase remains the same for $\phi = 0$. Relating these phases to the spatial frequencies ϕ_0 and $\boldsymbol{\phi}_{\text{int}}$, we shall shift the sources prior to applying the VIT by multiplying the input signal by $\mathbf{P}_{\phi_0} = \text{diag}([1, e^{-j\phi_0}, \ldots, e^{-j(M-1)\phi_0}])$, so that the desired signal virtually impinges from 0° and no phase amplification is noticed. Therefore, the shift and transformation are applied to (1) leading to

$$\begin{aligned}\check{\mathbf{x}}(n) &= \mathbf{T}_{\text{vit}}\mathbf{P}_{\phi_0}\mathbf{a}(\theta_0)s(n) + \mathbf{T}_{\text{vit}}\mathbf{P}_{\phi_0}\mathbf{A}_{\text{int}}(\boldsymbol{\theta}_{\text{int}})\mathbf{s}_{\text{int}}(n) \\ &\quad + \mathbf{T}_{\text{vit}}\mathbf{P}_{\phi_0}\mathbf{n}^{(\text{c})}(n) \qquad (18)\\ &= \check{\mathbf{a}}(\theta_0)s(n) + \check{\mathbf{A}}_{\text{int}}(\boldsymbol{\theta}_{\text{int}})\mathbf{s}_{\text{int}}(n) + \check{\mathbf{n}}^{(\text{c})}(n). \qquad (19)\end{aligned}$$

The vector $\check{\mathbf{a}}(\theta_0)$ and the matrix $\check{\mathbf{A}}_{\text{int}}(\boldsymbol{\theta}_{\text{int}})$ still have a Vandermonde structure and $\check{\mathbf{n}}^{(\text{c})}(n)$ is still a colored noise with its original color changed by the VIT so that $\check{\mathbf{n}}^{(\text{c})}(n) = \mathbf{L}' \cdot \mathbf{n}(n)$ and $\mathbf{L}' = \mathbf{T}_{\text{vit}} \cdot \mathbf{P}_{\phi_0} \cdot \mathbf{L}$. As shown in [14], Eq. (16) does not change the amplitude of $\mathbf{v}$ at $\phi = 0$ but it is changed for $\phi \neq 0$. By setting $K < 1$ the amplitude away from 0° is diminished making the VIT to operate as a beamformer. Thus, the interference and noise not in the direction of the desired signal is reduced.

The noise can have most of its power close to the desired signal and thus only being partially removed by the VIT. Therefore, the usage of prewhitening is still needed. With the transformed noise correlation model, the HASP can now be directly applied using the estimate

$$\hat{\mathbf{L}}' = \mathbf{T}_{\text{vit}} \cdot \mathbf{P}_{\phi_0} \cdot \hat{\mathbf{L}}. \tag{20}$$

Fig. 4 summarizes the VIT-HASP process. First the noisy signal is shifted by $\mathbf{P}_{\phi_0}$. At step 2 the VIT is incorporated. After that, the signal is ready to pass through the modified HASP, where $\hat{\mathbf{L}}'$ is used in place of $\hat{\mathbf{L}}$. The result is a dewhitened data $\check{\mathbf{x}}^{[s]\prime}(n)$ to be used as input to the adaptive GSC algorithms. For details on the computation of $\mathbf{T}_{\text{vit}}$ we refer to [14].

4.3. Deterministic prewhitening (DP)

In Sections 4.1 and 4.2, the structure of the noise covariance matrix is unknown. However, for highly correlated environments and for known covariance structure, a deterministic prewhitening (DP) can be employed with the expense of one sensor as explained in [5]. In Fig. 5 signal-free samples are first inserted into the system in order to estimate the noise structure with its correlation level. With the noise structure and correlation level in step 2 of Fig. 5, we can build the prewhitening matrix in step 3 of Fig. 5. In

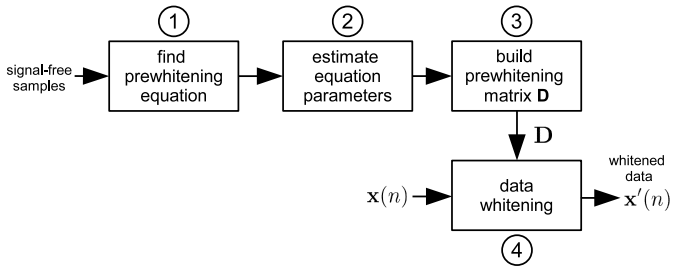

Fig. 5. Deterministic prewhitening diagram.

the last step the input data is multiplied by the generated matrix to produce the whitened data.

Here we assume that the noise is correlated as proposed by [19]:

$$n_{m+1}^{(\text{c})}(n) = \rho \cdot n_m(n) + \sqrt{1 - |\rho|^2} \cdot n_{m+1}(n), \tag{21}$$

where $0 \leqslant \rho < 1$ stands for the noise correlation coefficient. Once the noise correlation structure (21) is known, we can mount the correlation factor $\mathbf{L}$.

$$\mathbf{L}^{(\text{k})} = \begin{bmatrix} 1 & 0 & 0 & \cdots & 0 \\ \rho & \sqrt{1-|\rho|^2} & 0 & & 0 \\ \rho^2 & \rho\sqrt{1-|\rho|^2} & \sqrt{1-|\rho|^2} & \ddots & 0 \\ \vdots & \vdots & \vdots & & \vdots \\ \rho^{M-1} & \rho^{M-2}\sqrt{1-|\rho|^2} & \rho^{M-3}\sqrt{1-|\rho|^2} & \cdots & \sqrt{1-|\rho|^2} \end{bmatrix}. \tag{22}$$

For the known correlation structure we insert the superscript (k). The goal is to find a matrix $\mathbf{D}$ that will decorrelated the noise. In this work, we assume the same structure of the noise as shown in [5]. Therefore, the prewhitening matrix is given by

$$\mathbf{D} = \mathbf{J}_2 \cdot -\rho \cdot \mathbf{J}_1, \tag{23}$$

where $\mathbf{J}_2$ and $\mathbf{J}_1$ are the selection matrices $[\mathbf{0}_{(M-1)\times 1}\ \mathbf{I}_{M-1}]$ and $[\mathbf{I}_{M-1}\ \mathbf{0}_{(M-1)\times 1}]$ for the last $M-1$ sensors and the first $M-1$ sensors, respectively. By applying the matrix $\mathbf{D}$ on the colored noise matrix, the prewhitened noise becomes white but with a smaller power proportional to the factor $\sqrt{1-|\rho|^2}$.

$$\begin{aligned}\mathbf{N}' &= \mathbf{D} \cdot \mathbf{N}^{(\text{c})} = \mathbf{D} \cdot \mathbf{L}^{(\text{k})} \cdot \mathbf{N} \qquad (24)\\ &= \mathbf{J}_2 \cdot \mathbf{L}^{(\text{k})} \cdot \mathbf{N} - \rho \cdot \mathbf{L}^{(\text{k})} \cdot \mathbf{J}_1 \qquad (25)\\ &= \sqrt{1-|\rho|^2} \cdot \mathbf{J}_2 \cdot \mathbf{N}. \qquad (26)\end{aligned}$$

Eq. (24) shows that the noise is not only white but has its variance reduced. The matrix $\mathbf{J}_2$ on the last line of (24) shows the sacrifice of one sensor as a cost for the dewhitening. For applying the DP the whole data vector is multiplied by the DP matrix. This results in the prewhitened input data vector

$$\mathbf{x}'(n) = \mathbf{D} \cdot \mathbf{x}(n). \tag{27}$$

4.4. Block-wise reduced rank stochastic gradient GSC (BW-RR-SG-GSC)

In this subsection we show an alternative way to compute the reduced rank GSC beamformer by using the whole information contained in one block to estimate the expected values and correlation matrices. The objective of doing block-wisely computations is to reduce computational complexity in the prewhitening steps. The prewhitening requires the computation of the SVD, as seen in Section 4.1, and computing the GSC in blocks reduces the amount of SVDs to one per block.

Table 1
Computational costs in flops.

Algorithm	Cost
LMS-GSC, Section 3.1	$4M^2+4M-4$
RR-LMS-GSC, Section 3.2	$8M^2+4M+14Mr-10r+2$
DP-LMS-GSC, Sections 3.1 and 4.3	$6M^2+2M-4$
HASP-LMS-GSC, Sections 3.1 and 4.1	$8M^2N+2dMN+22N^3+2dM+4M^2+4M-4$
VIT-HASP-LMS-GSC, Sections 4.2 and 3.1	$8M^2N+2dMN+22N^3+2dM+4M^2+4M-4$
DP-RR-LMS-GSC, Sections 3.2 and 4.3	$10M^2+2M+14Mr-10r+2$
HASP-RR-LMS-GSC, Section 3.1 and 4.1	$8M^2N+22N^3+2dMN+2dM+8M^2+4M+14Mr-10r+2$
BW-RR-LMS-GSC, Section 4.4	$8M^2+8Mr+4MN+2M-6r-2N$
VIT-HASP-RR-LMS-GSC, Sections 3.2 and 4.2	$8M^2N+22N^3+2dMN+2dM+8M^2+4M+14Mr-10r+2$
HASP-BW-RR-LMS-GSC, Sections 4.1 and 4.4, i_b iterations per block	$\frac{1}{i_b}\cdot(8M^2N+22N^3+2dMN+2dM)+\frac{i_b}{N}\cdot(8M^2+8Mr+4MN+2M-6r-2N)$
VIT-HASP-BW-RR-LMS-GSC, Sections 4.2 and 4.4, i_b iterations per block	$\frac{1}{i_b}\cdot(8M^2N+22N^3+2dMN+2dM)+\frac{i_b}{N}\cdot(8M^2+8Mr+4MN+2M-6r-2N)$
HASP-BW-RR-LMS-GSC, Sections 4.1 and 4.4, N iterations per block	$16M^2+22N^2+2dM+2dM/N+8Mr+4MN+2M-6r-2N$
VIT-HASP-BW-RR-LMS-GSC, Sections 4.2 and 4.4, N iterations per block	$16M^2+22N^2+2dM+2dM/N+8Mr+4MN+2M-6r-2N$

First we define the CM input signal block as

$$\tilde{\mathbf{X}}_m = \mathbf{X}_m \cdot \mathrm{diag}(\mathbf{e}_m), \tag{28}$$

where $\mathbf{X}_m = \mathbf{X}(mN)$, $\mathbf{e}_m = [e_{\mathrm{rr}}(N(m-1)+1), \ldots, e_{\mathrm{rr}}(mN)]^{\mathrm{H}}$ and m denotes the block index. The previous definitions are used to write the estimates of the covariance matrix and expected values $\tilde{\mathbf{x}}(n)$

$$\hat{\mathbf{R}}_{\tilde{\mathbf{x}}\tilde{\mathbf{x}}} = \frac{1}{L}\tilde{\mathbf{X}}_m\tilde{\mathbf{X}}_m^{\mathrm{H}}, \tag{29}$$

$$\hat{\mathrm{E}}\{\tilde{\mathbf{x}}\} = \frac{1}{L}\tilde{\mathbf{X}}_m \cdot \mathbf{1}_N, \tag{30}$$

where $\mathbf{1}_N$ is a column vector of ones of length N. Inserting the estimates into the gradient of (9), one can write the stochastic gradient (SG) for both $\mathbf{T}$ and $\overline{\mathbf{w}}$:

$$\hat{\nabla}_{\mathbf{T}} J_{\mathrm{cm}} = -\frac{2}{L}\mathbf{B}\tilde{\mathbf{X}}_m(\mathbf{e}_m + \mathbf{1}_L)\overline{\mathbf{w}}^{\mathrm{H}}, \tag{31}$$

$$\hat{\nabla}_{\overline{\mathbf{w}}} J_{\mathrm{cm}} = -\frac{2}{L}\mathbf{T}^{\mathrm{H}}\mathbf{B}\tilde{\mathbf{X}}_m(\mathbf{e}_m + \mathbf{1}_N). \tag{32}$$

By defining an incremented error $\mathfrak{e}_m = \mathbf{e}_m + \mathbf{1}_N$, Eqs. (31) and (32) can be further simplified to generate the BW-RR-SG-GSC update rules (33) and (34).

$$\mathbf{T}(n+1) = \mathbf{T}(n) + \mu_T\tilde{\mathbf{X}}_B\mathfrak{e}_m\overline{\mathbf{w}}^{\mathrm{H}}, \tag{33}$$

$$\overline{\mathbf{w}}(n+1) = \overline{\mathbf{w}}(n) + \mu_w\mathbf{T}^{\mathrm{H}}\tilde{\mathbf{X}}_B\mathfrak{e}_m, \tag{34}$$

where $\tilde{\mathbf{X}}_B = \mathbf{B}\tilde{\mathbf{X}}_m$. The VIT and prewhitening schemes depicted in Sections 4.1–4.3 work in the same manner for the block-wise algorithm. The only difference is that the whole data from the output matrix is used in the HASP and VIT-HASP solutions.

4.5. Computational complexity analysis

In this subsection we compare the computational complexities of the classical and proposed solutions. We consider sums and multiplications for the computation of the complexity cost. The sum of the total amount of sums and multiplications are considered flops, which is the used measure unity [20]. In previous works [8,11], tables with a number of additions and multiplications are given for various GSC adaptive algorithms. Table 1 shows the complexity per sample of the used algorithms computed using the criteria and methods found in [20].

The LMS-GSC and BW-RR-LMS-GSC algorithms in Table 1 have no colored noise treatment and have a quadratic number of operations. By using a DP we add one matrix vector operation resulting in $2M^2-2M$ flops, thus keeping the quadratic complexity as seen in lines DP-LMS-GSC and DP-LMS-GSC. However, when the HASP algorithms are used, the SVD and a few matrix multiplications are required. This means that the computational cost becomes cubic. The SVD alone costs $4M^2N+22N^3$ [20].

The BW-RR-LMS-GSC alleviates the SVD cost effect. Since the filter is updated block-wisely, only one SVD per block is needed. If we set i_b iterations per block, then one should process in average i_b/N SVDs per sample. In schemes HASP-BW-RR-LMS-GSC and VIT-HASP-BW-RR-LMS-GSC in Table 1, if we choose $i_b = N$, the cubic factors vanish reducing drastically the computational cost.

5. Simulations and results

For the simulations, a ULA with 32 elements was considered and random uniformly distributed QAM signals with unitary l^2-norm for seven sources were generated, one relative to desired signal positioned and six relative to the interferes. The source and interferes are positioned at 10°, −63°, −43°, −21°, 28°, 39° and 61°, respectively. For all simulations, 600 samples were generated. Also, white Gaussian noise is added according to (1) and is latter correlated by using the structure seen in (22). The correlation is set to $\rho = 0.9$ and the signal to noise ratio (SNR) is fixed at 10 dB. The reduced rank is set to $r = 10$ and the results are evaluated according to the mean normalized error (MNE):

$$\mathrm{MNE}(n) = \frac{\mathrm{E}\{|s(n)-\hat{s}(n)|\}}{\mathrm{E}\{|s(n)|\}}. \tag{35}$$

Table 2 summarizes the notation used in the legends of figures of this section. It is worth noting that by default colored noise is used. When white Gaussian noise is used the term “white noise” is written after the abbreviation.

The results are shown in a Monte Carlo fashion after 1000 trials. For comparison we draw the MNE for the LMS-GSC in both white and colored noise. The Standard LMS-GSC is used since to the best of our knowledge there is no state-of-the-art beamformer for colored noise environments. Moreover, we assumed that the noise structure is given by (22). Previous works consider noise as directional interference [21,22] or beamformers designed with known interference direction [23]. The step size is set to $\mu_{\mathrm{lms}} = 0.0006$ in order to give a similar curves as in [8,11] and yet not to diverge in colored noise scenarios. The same μ_{lms} is adopted for the other simulations in this section. This same approach is used for step size choice in the other simulations seen in this section. The optimization of μ_{lms} for colored noise scenarios is a topic for a future work. Results for the LMS-GSC algorithms are seen in Fig. 6.

Note, in Fig. 6, the degradation of performance of the LMS-GSC white noise to the LMS-GSC. The only difference between both curves is that in LMS-GSC white noise, the noise correlation is 0 and, in LMS-GSC, the noise correlation is 0.9. If noise-only samples are available, the proposed HASP solution represented by the dark blue curve can be used. The MNE of the HASP-LMS-GSC scheme

Table 2
Notation of the legends used in the figures.

Abbreviation	Description
Batch GSC white noise	State-of-the-art GSC using all samples to estimate **w** in a white noise scenario
LMS-GSC white noise	State-of-the-art adaptive GSC in a white noise scenario
LMS-GSC	State-of-the-art adaptive GSC in a colored noise scenario
Proposed DP-LMS-GSC	Adaptive GSC with deterministic prewhitening in a colored noise scenario
Proposed HASP-LMS-GSC	Adaptive GSC with high accuracy stochastic prewhitening in a colored noise scenario
Proposed VIT-HASP-LMS-GSC	Adaptive GSC with Vandermonde invariance transformation based high accuracy stochastic prewhitening in a colored noise scenario
RR-LMS-GSC white noise	State-of-the-art reduced rank adaptive GSC in a white noise scenario
RR-LMS-GSC	State-of-the-art reduced rank adaptive GSC in a colored noise scenario
HASP-RR-LMS-GSC	Adaptive reduced rank GSC with high accuracy stochastic prewhitening in a colored noise scenario
VIT-HASP-RR-LMS-GSC	Adaptive reduced rank GSC with Vandermonde invariance transformation based high accuracy stochastic prewhitening in a colored noise scenario
Proposed BW-RR-LMS-GSC white noise	Block-wise reduced rank adaptive GSC in a white noise scenario
Proposed HASP-BW-RR-LMS-GSC	Block-wise reduced rank adaptive GSC with high accuracy stochastic prewhitening in a colored noise scenario
Proposed VIT-HASP-BW-RR-LMS-GSC	Block-wise reduced rank adaptive GSC with Vandermonde invariance transformation based high accuracy stochastic prewhitening in a colored noise scenario

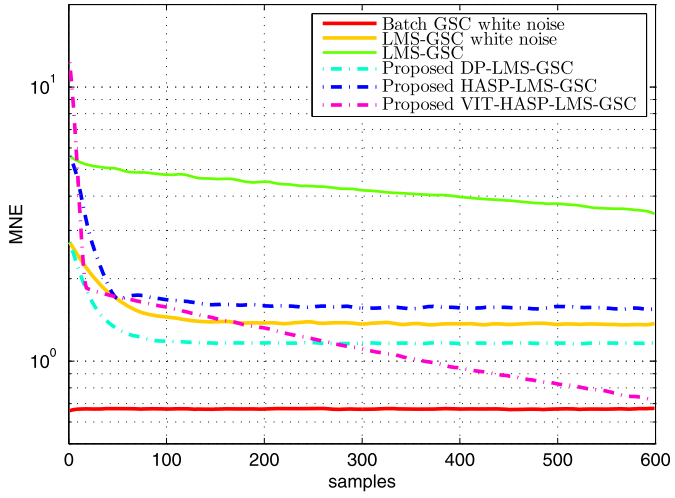

Fig. 6. MNE of the LMS-GSC type algorithms versus samples for $N = 50$ and an SNR of 10 dB.

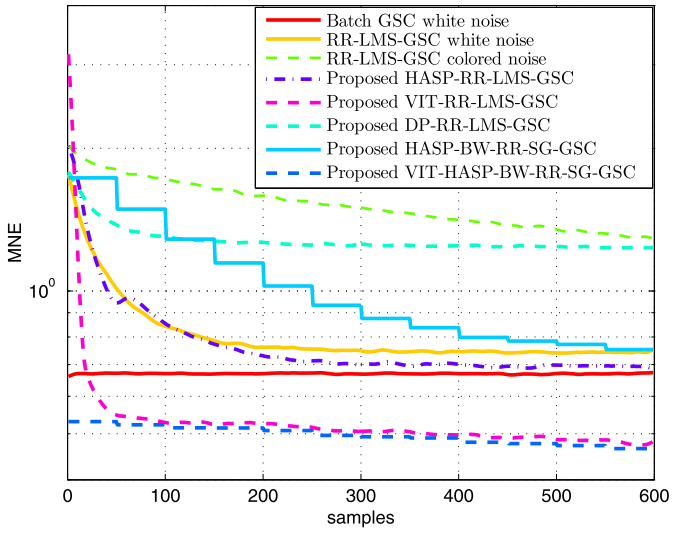

Fig. 7. MNE of the RR-LMS-GSC type algorithms versus samples for $N = 50$ and an SNR of 10 dB.

is drastically reduced in comparison with the standard LMS-GSC. For a VIT-HASP solution an even further reduction of MNE can be observed. For comparison we plot the batch GSC solution, i.e. the non-adaptive solution using all the samples to estimate beamforming filter [9]. As the system evolves in time, the proposed VIT-HASP-LMS-GSC, which run in colored noise scenario, almost reaches the batch GSC white noise curve. Applying the proposed DP-LMS-GSC for a known correlation structure makes the algorithm performs better than in a white noise environment, since the noise is reduced.

In Fig. 7, we rerun the simulations for the RR algorithms. The step sizes are set to $\mu_{\overline{w}} = 0.0001$ and $\mu_T = 0.00001$. Also the standard RR-LMS-GSC is used for comparison. For the block-wise algorithm we have $\mu_{\overline{w}} = 0.0001/N$ and $\mu_T = 0.00001/N$. For the VIT-HASP schemes the step sizes were slightly decreased to $\mu_{\overline{w}} = 0.00005$ and $\mu_T = 0.000008$ for sake of implementation stability. In Fig. 7, it is also seen that even though the RR schemes have a superior overall performance, the colored noise provokes a large reduction of performance and shows a clear necessity of whitening the noise. The deterministic prewhitening has a positive, but not large, effect by decreasing MNE. The proposed HASP-RR-LMS-GSC was shown to outperform the other methods. The combined VIT-HASP-RR-LMS-GSC has an even smaller MNE outperforming the HASP-RR-LMS-GSC.

Since the SVD increases significantly the computational complexity of the algorithms using a HASP solution, the BW-RR-SG-GSC is also shown as an alternative when computational power is not sufficiently available. The computational savings come at the cost of response time. The block size is chosen to $N = 50$ and the number of iterations within each block is $2 \cdot N$. Even though a slower convergence is noticed, the HASP-BW-RR-SG-GSC gets close to the HASP-RR-LMS-GSC on the final MNE. Also, the VIT plays an important role in reducing the MNE. As shown in Fig. 7, the VIT does most of the filtering task and the gain of the adaptive GSC becomes smaller. The steep descent seen on the first 50 samples of the VIT-HASP-RR-LMS-GSC curve is basically due the data length when performing the low rank approximation. Once the data reaches its limit, here set to 50, the MNE remains almost constant.

In Fig. 8 we compare the BW-RR-SG-GSC white noise scenarios with the HASP-BW-RR-LMS-GSC and the VIT-HASP-BW-RR-LMS-GSC. The HASP-RR-LMS-GSC and the VIT-HASP-RR-LMS-GSC curves are left for reference. The BW-RR-SG-GSC does not improve MNE in a colored noise scenario with $\rho = 0.9$. In Fig. 8, the HASP-BW-RR-SG-GSC has a similar performance when compared to the BW-RR-SG-GSC in a white noise environment and the VIT-HASP-BW-RR-LMS-GSC has a similar MNE to the VIT-HASP-RR-LMS-GSC.

In Fig. 9 the evolution of the MNE in terms of block size is shown for the full rank algorithms. The HASP-LMS-GSC has a better performance than the DP-LMS-GSC when $N > 80$ and the VIT-HASP-LMS-GSC has its performance almost unchanged for $N > 50$.

In Fig. 10 the evolution of the MNE in terms of block size is shown for the reduced rank algorithms. As shown in Fig. 10, the

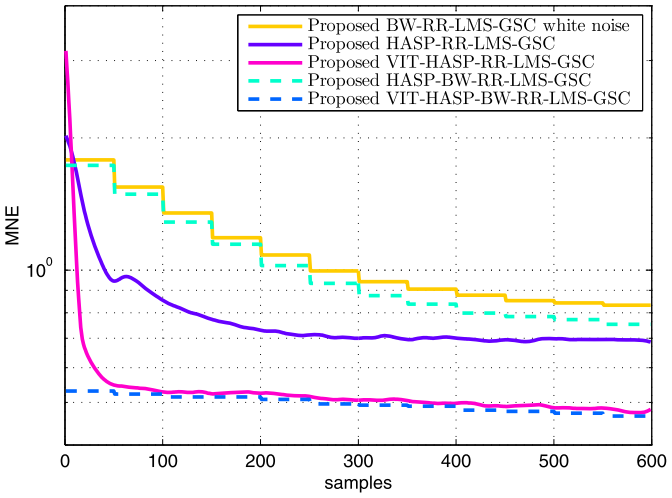

Fig. 8. MNE in dB for LMS-GSC type algorithms with a varying N and an SNR of 10 dB.

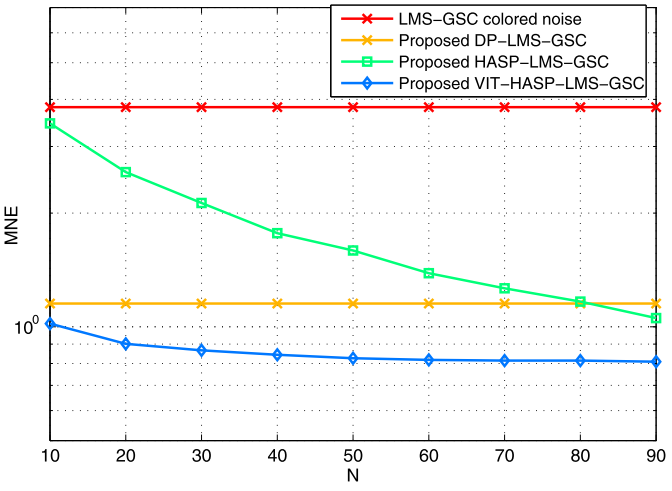

Fig. 9. MNE in dB for LMS-GSC type algorithms with a varying N and an SNR of 10 dB.

block size plays an important role in the reduced rank algorithms, specially for the HASP-only prewhitening schemes. The VIT based HASP algorithm has the best performance in comparison to the other schemes.

6. Conclusion

In this paper, we have extended the adaptive GSC and the reduced rank adaptive GSC for colored scenarios. As shown in this work, the colored noise degrades significantly the performance of the GSC and RR-GSC algorithms. To reduced MNE in these scenarios, we proposed the DP-LMS-GSC, the HASP-LMS-GSC and the VIT-HASP-LMS-GSC algorithms for the full rank adaptive GSC and the DP-RR-LMS-GSC, HASP-RR-LMS-GSC and VIT-RR-LMS-GSC for the reduced rank adaptive GSC. These algorithms are based on the DP, on the stochastic prewhitening and on the VIT. The DP is used when the correlation structure of the noise is known and the stochastic prewhitening when it is unknown. The VIT acts as a pre-beamformer reducing the power that is not in direction of the desired signal.

The stochastic prewhitening requires one SVD to be computed at each sample. To reduce the number of SVD computations, a block-wise SG-RR-GSC was proposed. The algorithm adapts its

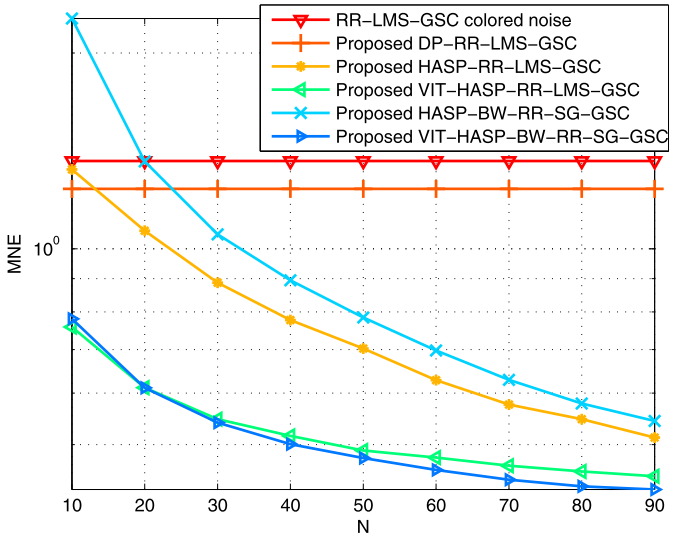

Fig. 10. MNE in dB for LMS-GSC type algorithms with a varying N and an SNR of 10 dB.

filter block by block making only one SVD per block necessary reducing computational cost. The block-wise SG-RR-GSC in colored noise scenarios led to the development of the HASP-BW-RR-SG-GSC and VIT-BW-RR-SG-GSC algorithms.

The incorporation of prewhitening schemes transforms back the colored noise into white noise allowing a significant improvement of the GSC and RR-GSC. Based on that, several algorithms were proposed for colored noise scenarios. A block-wise algorithm was proposed to reduced the number of SVD computations to one per block. By means of simulation, a lower MNE was achieved in the final result when compared to the sample-wise methods.

Acknowledgments

The authors would like to thank the Foundation for Research Support of the Brazilian Federal District (FAPDF) under the process number 193.000.903/2013, the Coordination for the Improvement of Higher Education Personnel (CAPES) and the National Council for Scientific and Technological Development (CNPq) under the process number 88881.030392/2013-01 for their financial support on this research. The authors would also like to thank the head editor and reviewers for their valuable comments and suggestions for improving this paper's quality.

Appendix A. Supplementary material

Supplementary material related to this article can be found online at http://dx.doi.org/10.1016/j.dsp.2014.07.015.

References

[1] Z. Yang, R.C. de Lamare, X. Li, L1 regularized STAP algorithm with a generalized sidelobe canceler architecture for airborne RADAR, in: 2011 IEEE Statistical Signal Processing Workshop, Jun. 2011, pp. 329–332.
[2] J.E. Thorner, Approaches to SONAR beamforming, in: Proc. of Southern Tier Technical Conference, Apr. 1990, pp. 69–78.
[3] K. Mori, H. Arai, Y. Qian, T. Itoh, Direct conversion receiver for digital beamforming at 8.45 GHz, in: Proc. of 2001 IEEE MTT-S International Microwave Symposium, vol. 2, May 2001, pp. 1375–1378.
[4] W. Herbordt, W. Kellermann, Adaptive Beamforming for Audio Signal Acquisition, Springer, 2003, pp. 155–194.
[5] J.P.C.L. da Costa, F. Roemer, M. Haardt, Deterministic prewhitening to improve subspace parameter estimation techniques in severely colored noise environments, in: Proc. of 54th International Scientific Colloquium (IWK'09), Ilmenau, Germany, Sept. 2009.

[6] M. Haardt, R.S. Thomä, A. Richter, Multidimensional high-resolution parameter estimation with applications to channel sounding, in: Y. Hua, A. Gershman, Q. Chen (Eds.), High-Resolution and Robust Signal Processing, Marcel Dekker, New York, NY, 2004, pp. 255–338, Chapter 5.
[7] J.P.C.L. da Costa, Parameter Estimation Techniques for Multi-Dimensional Array Signal Processing, Shaker Publisher, Aachen, Germany, Mar. 2010.
[8] L. Wang, Array signal processing algorithms for beamforming and direction finding, Ph.D. dissertation, University of York, 2009.
[9] S. Haykin, Adaptive Filter Theory, 3rd edition, Prentice-Hall, 1996.
[10] S.J. Chern, C.H. Sun, C.C. Chang, Blind adaptive DS-CDMA receivers with sliding window constant modulus GSC-RLS algorithm, in: International Symposium on Intelligent Signal Processing and Communications, ISPACS'06, Dec. 2006, pp. 979–982.
[11] L. Wang, R.C. de Lamare, M. Yukawa, Adaptive reduced-rank constrained constant modulus algorithms based on joint iterative optimization of filters for beamforming, IEEE Trans. Signal Process. 58 (Jun. 2010) 2983–2997.
[12] P.C. Hansen, S.H. Jensen, Prewhitening for rank-deficient noise in subspace methods for noise reduction, IEEE Trans. Signal Process. 53 (Oct. 2005) 3718–3726.
[13] J.P.C.L. da Costa, K. Liu, H.C. So, F. Roemer, M. Haardt, S. Schwarz, Multidimensional prewhitening for enhanced signal reconstruction and parameter estimation in colored noise with Kronecker correlation structure, Signal Process. 93 (11) (Nov. 2013) 3209–3226, Elsevier publisher.
[14] M.T. Ivrlac, T.P. Kupjuhn, J.A. Nossek, Vandermonde invariance transformation, in: Proc. ICASSP 2001, vol. 5, Salt Lake City, USA, May 2001, pp. 2929–2932.
[15] J.P.C.L. da Costa, F. Roemer, R.T. de Souza Jr., Enhanced Model Order Estimation in Colored Noise Scenarios via Noise Prewhitening, in: XXIX Simpósio Brasileiro de Telecomunicações (SBrT'11), Curitiba, Brazil, October 2011, http://www.dee.ufma.br/~fsouza/Anais_SBrT_2011/prog_2.html.
[16] J.P.C.L. da Costa, A. Thakre, F. Roemer, M. Haardt, Comparison of model order selection techniques for high-resolution parameter estimation algorithms, in: Proc. 54th International Scientific Colloquium (IWK), Ilmenau, Germany, Sept. 2009.
[17] J.P.C.L. da Costa, F. Roemer, M. Haardt, R.T. de Sousa Jr., Multi-dimensional model order selection, EURASIP J. Adv. Signal Process. 26 (20 July 2011), Springer publisher.
[18] M.A.M. Marinho, F. Antreich, J.P.C.L. da Costa, J.A. Nossek, A signal adaptive array interpolation approach with reduced transformation bias for DOA estimation of highly correlated signals, in: IEEE International Conference on Acoustics, Speech, and Signal Processing (ICASSP), Florence, May 2014.
[19] Y.H. Chen, Y.S. Lin, DOA estimation by fourth-order cumulants in unknown noise environments, in: Proc. of IEEE ICASSP-93, vol. 4, Minneapolis, USA, Apr. 1993, pp. 296–299.
[20] G.H. Golub, Charles F. Van Loan, Matrix Computations, JHU Press, 1996.
[21] S. Affes, S. Gazor, Y. Grenier, An algorithm for multisource beamforming and multi-target tracking, IEEE Trans. Signal Process. 44 (1996) 1512–1522.
[22] J.R. Mohammed, A new robust adaptive beamformer for enhancing speech corrupted with colored noise, in: Proc. International Conference on Computer Systems and Applications, AICCSA 2008, 2008, pp. 508–515.
[23] Z. Linrang, B. Zheng, L. Guisheng, Adaptive beamforming in colored noise environment, in: Proc. International Conference on Signal Processing Proceedings, ICSP'98, 1998, pp. 343–346.

Ricardo Kehrle Miranda received the Diploma degree in telecommunications engineering in 2010 and the M.Sc. degree in electronic and automation systems in 2013 both from the University of Brasília (UnB), Brazil. In Germany, he did part of his M.Sc. work at the University of Erlangen–Nuremberg and was as visitor student at the German Aerospace Center (DLR). Currently, he pursues a Ph.D. degree at the UnB with interests on array signal processing and navigation.

João Paulo C.L. da Costa received the Diploma degree in electronic engineering in 2003 from the Military Institute of Engineering (IME) in Rio de Janeiro, Brazil, his M.Sc. degree in 2006 from University of Brasília (UnB) in Brazil, and his Doktor-Ingenieur (Ph.D.) degree with Magna cum Laude in 2010 at Ilmenau University of Technology (TU Ilmenau) in Germany. Since 2010, he coordinates the Laboratory of Array Signal Processing (LASP) and since 2011, he works as a senior researcher at the Ministry of Planning in projects related to Business Intelligence. He was a visiting scholar and professor at University Erlangen–Nuremberg, at Munich Technical University, at University of Seville and at Harvard University. Currently he coordinates a project related to on-line courses at the National School of Public Administration (ENAP) and a special visiting researcher (PVE) project related to satellite communication and navigation together with the German Aerospace Center (DLR) supported by the Brazilian government.

Felix Antreich received the Diploma degree in electrical engineering from the Munich University of Technology (TUM), Munich, Germany, in 2003. In 2011 he received the Doktor-Ingenieur (Ph.D.) degree also from the TUM. Since July 2003, he has been an Associate Researcher with the Department of Navigation, Institute of Communications and Navigation of the German Aerospace Center (DLR), Wessling-Oberpfaffenhofen. He also is a Special Visiting Researcher (PVE) at the University of Brasília (UnB) within the Programa Ciência sem Fronteiras funded by CAPES and CNPq. His research interests include sensor array signal processing for global navigation satellite systems (GNSS) and wireless communications, estimation theory and signal design for synchronization, and GNSS.